

Long-term foehn reconstruction combining unsupervised and supervised learning

Reto Stauffer 
Universität Innsbruck

Achim Zeileis 
Universität Innsbruck

Georg J. Mayr 
Universität Innsbruck

Abstract

Foehn winds, characterized by abrupt temperature increases and wind speed changes, significantly impact regions on the leeward side of mountain ranges, e.g., by spreading wildfires. Understanding how foehn occurrences change under climate change is crucial. Unfortunately, foehn cannot be measured directly but has to be inferred from meteorological measurements employing suitable classification schemes. Hence, this approach is typically limited to specific periods for which the necessary data are available.

We present a novel approach for reconstructing historical foehn occurrences using a combination of unsupervised and supervised probabilistic statistical learning methods. We utilize in-situ measurements (available for recent decades) to train an unsupervised learner (finite mixture model) for automatic foehn classification. These labeled data are then linked to reanalysis data (covering longer periods) using a supervised learner (lasso or boosting). This allows to reconstruct past foehn probabilities based solely on reanalysis data.

Applying this method to ERA5 reanalysis data for six stations across Switzerland and Austria achieves accurate hourly reconstructions of north and south foehn occurrence, respectively, dating back to 1940. This paves the way for investigating how seasonal foehn patterns have evolved over the past 83 years, providing valuable insights into climate change impacts on these critical wind events.

Keywords: Foehn, reconstruction, unsupervised, mixture model, supervised, climate, trend.

1. Introduction

Foehn winds are downslope winds on the leeward side of mountains and can be found all around the world in areas with pronounced topographical features that impede the airflow, such as the European Alps, the Southern Alps in New Zealand, mountain ranges along the Mediterranean Sea, or the Rocky Mountains. Depending on the region, these winds are given specific names such as Santa Anna winds (Southern California), Chinook (Rocky Mountains), Mistral (Southern France), Bora (Croatia), or Foehn (Central Europe and New Zealand). For historical reasons ‘foehn’ has become a synonym for this type of terrain-induced wind phenomena.

Often, foehn is characterized by a sharp increase in wind speed and sudden changes in temperature and relative humidity, which can have a strong influence on the local climate and the people living in the affected areas. While foehn is often associated with a mild (and typically dry) climate, strong foehn events can also cause extensive damage to vegetation and

man-made structures. In some areas it is not uncommon for strong foehn gusts to overturn trucks or vans, or for airports and harbors to be closed due to unsafe conditions. In addition, the strong and dry winds can kindle and spread domestic fires and wild fires (Schoennagel, Veblen, and Romme 2004; Reinhard, Rebetez, and Schlaepfer 2005; Zumbrunnen, Bugmann, Conedera, and Bürgi 2009) or affect the development of Antarctic ice shelves (e.g., Cape, Vernet, Skvarca, Marinsek, Scambos, and Domack 2015; Elvidge, Kuipers Munneke, King, Renfrew, and Gilbert 2020).

Although the conceptual model of foehn is well established (Armi and Mayr 2007; Mayr and Armi 2008; Armi and Mayr 2011; Richner and Hächler 2013), it cannot be measured directly. During the last decades several (semi)-automatic methods have been developed which allow to differentiate ‘foehn’ and ‘no-foehn’ events based on in-situ measurements from automated weather stations (AWSs). Among the frequently used algorithms are Widmer’s föhn index (Widmer 1966; Courvoisier and Gutermann 1971) based on Fisher’s linear discriminant analysis to distinguish between two or more distinct classes, and enhanced versions of it (e.g., Jansing, Papritz, Dürr, Gerstgrasser, and Sprenger 2022). Other studies use decision-based or tree-based methods to classify foehn events (e.g., Dürr 2008; Speirs, McGowan, Steinhoff, and Bromwich 2013; Cape *et al.* 2015; Turton, Kirchgaessner, Ross, and King 2018; Datta *et al.* 2019; Elvidge *et al.* 2020; Laffin, Zender, Singh, Van Wessem, Smeets, and Reijmer 2021; Francis, Fonseca, Mattingly, Lhermitte, and Walker 2023; Laffin *et al.* 2021; Francis *et al.* 2023), all of which are deterministic methods, where the thresholds have often been selected manually. To overcome these limitations, Plavcan, Mayr, and Zeileis (2014) proposed a method based on finite mixture models for automatic and fully parametric probabilistic foehn classification. To perform the classification, all methods require AWS measurements with high temporal resolution (ideally sub-hourly), which are typically only available for recent decades. While this allows to classify and analyze foehn when the AWS provides sufficient data, there is no information on foehn prior to the installation of the AWS, nor when there have been outages or the AWS has been decommissioned.

Additional information on the atmospheric conditions from numerical (re-)analysis models are an excellent source to complement the in-situ measurements. Reanalysis data sets are typically produced by physically based numerical weather prediction (NWP) models and sophisticated data assimilation schemes that use all available observations to estimate the ‘best known’ atmospheric state. An example is the global reanalysis data set ERA5 (Hersbach *et al.* 2023a,b) from the European Centre for Medium-Range Weather Forecasts (ECMWF). ERA5 provides global hourly 4-dimensional atmospheric conditions back to 1940. However, this comes with its own challenges. First, foehn is not explicitly modeled by the NWP models. Second, due to technical and computational limitations, the reanalysis can only approximate the real world and cannot resolve small-scale atmospheric processes and topographic features, which would be important for small-scale phenomena such as foehn.

One way to overcome these limitations is to combine AWS measurements and reanalysis data using statistical or machine learning techniques. A classification of foehn based on AWS data serves as the response (target/outcome/labels) for a supervised model that uses reanalysis data as explanatory variables (inputs/covariates). Once the relationship between the two sets of data has been learned, the models can be used to predict the expected state (‘foehn’ or ‘no foehn’) for periods for which reanalysis data is available but AWS measurements are not. This is also known as (statistical) downscaling or post-processing and has been used for foehn modeling in some variations: For nowcasting foehn at a station in Switzerland (Altdorf),

Sprenger, Schemm, Oechslin, and Jenkner (2017) use data from a local 7 km analysis data set (COSMO-7) – but only to get consistent inputs for their adaptive boosting algorithm (AdaBoost). Laffin *et al.* (2021) use both ERA5 and the Regional Atmospheric Climate Model 2 (RACMO2; Wessen and Laffin 2022) combined with tree-based gradient boosting (XGBoost; Chen and Guestrin 2016) to predict foehn on the Antarctic Peninsula. XGBoost is also used by Mony, Jansing, and Sprenger (2021) to investigate future changes to foehn frequency in Switzerland.

This study proposes a novel probabilistic approach that combines unsupervised and supervised machine learning methods to bridge the gap between in-situ Automatic Weather Station (AWS) measurements and ERA5 reanalysis data to diagnose foehn. This combined approach allows us to reconstruct long-term, high-resolution foehn conditions over several decades. ERA5 data enables us to reconstruct the probability of foehn occurrence with hourly temporal resolution dating back to 1940, long before AWS were installed.

Our approach also allows to identify potential long-term changes in foehn occurrence in the European Alps from this high-resolution reconstruction. The validity of this combined approach is demonstrated by applying it to six stations located both north and south of the main Alpine ridge to show the method’s effectiveness for both north and south foehn wind situations.

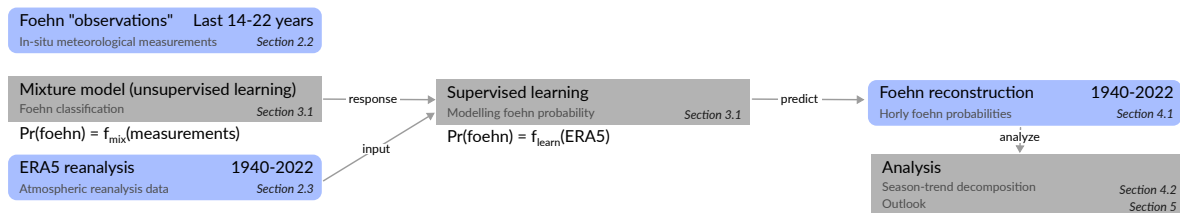


Figure 1: Flow chart for the new combined foehn reconstruction algorithm.

Figure 1 shows a schematic representation of the proposed approach. For all six locations, data are available from an AWS at the target location as well as from a nearby mountain station for the last 14–22 years (Sec. 2.1) on a 10 min temporal interval. A Gaussian mixture model (unsupervised learning; Sec. 3.1) is used for foehn classification. The result is then aggregated into binary time series (‘foehn’/‘no foehn’) with an hourly temporal resolution to match the resolution of the ERA5 data used in the next step. After combining the different data sources, supervised learning (Sec. 3.2) is used to find the relationship between a variety of interpolated and derived variables from ERA5 (Sec. 2.2) and the classified events. Once these statistical models have been estimated, foehn can be reconstructed (Sec. 3.3) for the whole period from 1940–2022, allowing to investigate possible trends and/or seasonal changes over the last decades (Sec. 3.4).

2. Data

Section 2.1 describes the measurement data utilized for foehn classification along with the study area and the target stations. Section 2.2 explains the reanalysis data set and its pre-processing for the supervised learning method, along with the reconstruction process.

2.1. In-situ measurements

This study utilizes data from six AWSs situated across Switzerland and the western part of Austria, all positioned at the bottom of valleys known to be affected by foehn winds. Four of these stations are located north of the main Alpine ridge, while two are located in the canton of Ticino (Switzerland) south of the main Alpine ridge. Whilst the stations north of the Alps are prone to south foehn, the stations south of the Alps are known for the presence of north foehn.

An additional AWS upstream near the crest of the main Alpine range improves the accuracy of the foehn classification (Plavcan *et al.* 2014). The stations Innsbruck and Ellbögen utilize data from Sattelberg, the remaining four stations in Switzerland use observations from station Gütsch.

All stations provide data on mean wind speed, wind direction, air temperature, and relative humidity at a 10 min temporal resolution. Table 1 displays the locations and data availability of these stations, while Figure 2 depicts a map illustrating their geographical position and the surrounding topography.

	Type	Location	Data availability
\triangle Gütsch (Andermatt) ¹	crest	46.653N/8.616E 2286m	2005-01-01–2023-12-31 (95.3%)
Altdorf ¹	south	46.890N/8.620E 438m	2005-01-01–2022-12-31 (78.1%)
Montana ¹	south	46.290N/7.460E 1423m	2005-01-01–2022-12-31 (77.1%)
Comprovasco ¹	north	46.460N/8.935E 576m	2005-01-01–2022-12-31 (85.8%)
Lugano ¹	north	46.004N/8.960E 205m	2005-01-01–2022-12-31 (90.2%)
\triangle Sattelberg ²	crest	47.011N/11.479E 2107m	2006-01-01–2022-12-31 (75.0%)
Ellbögen ²	south	47.200N/11.430E 1080m	2006-01-01–2022-12-31 (92.0%)
(Universität) Innsbruck ³	south	47.260N/11.385E 578m	2009-06-21–2022-12-30 (99.1%)

Table 1: Station type, location and data availability; begin and end date plus percent available within period. Observations provided by the Swiss national weather service (1; MeteoSwiss), the University of Innsbruck (2) and the Austrian national weather service (3; GeoSphere Austria). Four stations are used to model south foehn, two to model north foehn and two serving information at the mountain crest (\triangle ; cf. Type).

2.2. ERA5 reanalysis

This study makes use of ERA5 reanalysis data, which is publicly accessible via the Copernicus climate data store (Hersbach *et al.* 2023a,b). ERA5 offers four-dimensional gridded data with an hourly temporal resolution (starting from 1940) on a spatial grid of $0.25^\circ \times 0.25^\circ$ ($\sim 28 \text{ km} \times 20 \text{ km}$ for Central Europe).

The data from 90 different fields (30 single level fields and 60 pressure level fields; see App. A) are bilinearly interpolated to the geographical location of the six stations of interest. Based on the 90 interpolated values, a series of derived variables is calculated, including vertical temperature gradients and level thickness, resulting in a total of 155 variables. These 155 variables are referred to as the ‘direct’ variable set as they solely rely on information retrieved directly from the geographical location of the corresponding target station.

Since foehn is driven by large-scale synoptic processes, it might be insufficient to rely only on data at the target location. Therefore, additional information from the surrounding is incor-

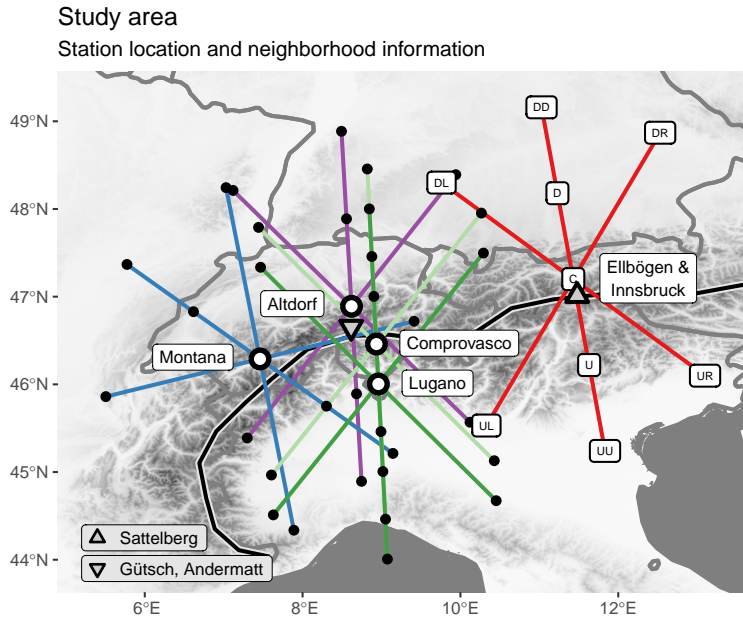


Figure 2: Location of the six target stations (circles/C) and two crest stations (triangles); Innsbruck and Ellbögen are shown combined due to their close proximity ($< 8 \text{ km}$). The solid black lines represents the main Alpine ridge. On top, the neighborhood ‘star’ used for interpolation is shown, exemplarily labeled on the most eastern station (details see App. A).

porated by extracting data from ERA5 at a series of neighboring points in a ‘star’ formation around the target location. In combination with the direct variables, a list of additional derived variables is calculated, such as spatial temperature differences and spatio-temporal pressure differences, among many others. Finally, the first and second order harmonics of the day of the year are included to capture seasonal variation. In total, this yields 497 variables: four harmonics, 155 direct variables, 136 spatial variables, 120 temporal variables and 82 spatio-temporal variables (e.g., temporal changes of spatial differences). This expanded set is referred to as the ‘full’ variable set.

Figure 2 shows the target locations (C; center) and their neighboring points used. These neighboring points are positioned geographically relative to the target station upstream (U) and downstream (D) of the main foehn wind direction as well as to the right (R) and left (L) of it. While the interpolated information from the target location itself (C) is always used as possible covariate for the statistical models, the values interpolated at the neighboring points are not directly employed but are instead used for the calculation of the derived/augmented variables. Further details regarding the construction of the neighboring ‘star’ can be found in Appendix A.

3. Methodology

Section 3.1 introduces the unsupervised learning model used for foehn classification, followed by the supervised learning models in Section 3.2. The results from Section 3.2 are then used to reconstruct hourly foehn occurrence over the past decades (Sec. 3.3) which is analyzed

employing season-trend decomposition in Section 3.4.

3.1. Unsupervised learning: Mixture model for foehn classification

As direct foehn measurement do not exist, the data from the AWSs are currently unlabeled. Therefore, a mixture model is employed to distinguish between the ‘foehn’ and ‘no foehn’ events:

$$\text{Pr}_{\text{obs}}(\text{foehn}) = f_{\text{mix}}(\text{measurements}). \quad (1)$$

$\text{Pr}_{\text{obs}}(\text{foehn})$ denotes the posterior probability for a ‘foehn’ observation at a specific time and station, which is modeled as a function ($f_{\text{mix}}()$) of the 10 min in-situ measurements (Sec. 2.1). We employ a two-component Gaussian mixture model (Grün and Leisch 2008) with concomitants, closely following the method proposed by Plavcan *et al.* (2014) implemented in the *R* package *foehnix* (Stauffer 2023).

The prerequisite condition for an observation to be used for classification is that the wind direction at the location of interest falls within the prevailing foehn direction at the target location, and that wind from a specific direction is also prevalent at the corresponding crest station at the same time (details in Tab. 4). Only the periods matching this precondition are used for estimating the Gaussian mixture model, while $\text{Pr}_{\text{obs}}(\text{foehn}) = 0$ is set for all remaining observations.

The underlying concept involves that two unobservable Gaussian components (or clusters) exist, one describing ‘foehn’ conditions and the other ‘no foehn’ conditions. To distinguish between these two components, a main covariate is required. In this study, the potential temperature difference ($\Delta\theta$) between the valley station (t_{valley}) and the crest station (t_{crest}) is used, employing a simple dry adiabatic temperature reduction $\Delta\theta = t_{\text{valley}} - t_{\text{crest}} - 0.01\Delta h$ based on the difference in altitude (Δh ; cf. Tab. 1 & 4). During foehn events, the air descends on the leeward side of the mountains, resulting in a well-mixed atmosphere with neutral stratification, hence a potential temperature difference close to zero.

However, the potential temperature difference alone might not be sufficient to adequately separate the two states. Therefore, an additional concomitant model is employed to weigh the two components conditional on additional covariates. In this study, binary logistic regression is used for the concomitant model, employing relative humidity and mean wind speed as additional covariates. Models with this specification have been shown to work well for stations in the Alpine region (e.g., Plavcan *et al.* 2014; Plavcan and Mayr 2015). Figure 3 provides an illustration of this model, depicting the use of $\Delta\theta$ to separate the two components (‘foehn’/‘no foehn’) and the effect of the concomitant model on the joint density. More details can be found in Appendix B.

Once estimated, the mixture model provides the posterior probability $\text{Pr}_{\text{obs}}(\text{foehn})$ for each 10 min interval where the required in-situ measurements are available (Eqn. 1). As these foehn ‘observations’ need to be combined with ERA5 in the next step, the results are upscaled to an hourly temporal resolution ($\text{Pr}_{1\text{h}}$). Therefore, the following basic assumption is applied: Each hour is considered a ‘foehn’ event if at least half of the 10 min posterior probabilities within that hour (e.g., 00:10–01:00 UTC for 01:00 UTC) are ≥ 0.5 , otherwise the hour is considered a ‘no foehn’ event. If fewer than 4 out of 6 individual 10 min probabilities are available, the hour is excluded. This is similar to Gutermann, Dürr, Richner, and Bader (2012) and Mony

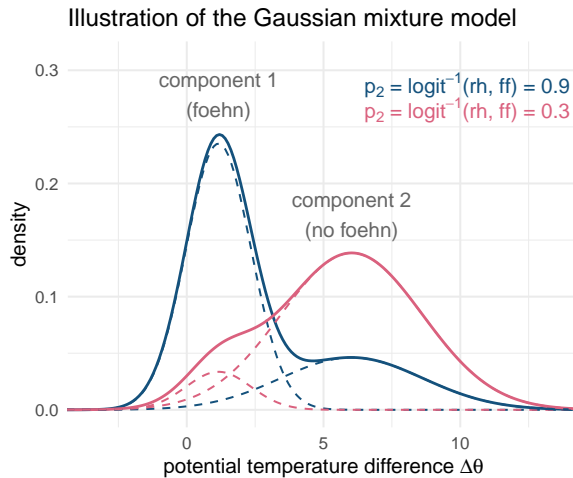


Figure 3: Illustration of the two-component Gaussian mixture model used for classification. The potential temperature difference ($\Delta\theta$) is used as the main variable to separate component 1 (foehn) and component 2 (no foehn); the concomitant model includes relative humidity (rh) and mean wind speed (ff) at the valley station. Solid lines: density of the mixture model once with a probability $p_2 = 0.9$ to observe component 2, once with $p_2 = 0.3$.

et al. (2021) who employ a ‘four out of six rule’.

$$\text{Pr}_{1h} = \begin{cases} \text{missing} & \text{if } \sum \text{Pr}_{\text{obs}} \in [0 - 1] < 4 \\ \text{foehn} & \text{if } \frac{1}{N} \sum (\text{Pr}_{\text{obs}} \geq 0.5) \geq 0.5 \\ \text{no foehn} & \text{else} \end{cases} \quad (2)$$

3.2. Supervised learning: Modeling foehn probability

The outcome of the previous section is a binary time series, with each hour labeled as either a ‘foehn’ or ‘no foehn’ observation (Eqn. 2). This serves as the response variable in the supervised machine learning model, using the ERA5 data (Sec. 2.2) as input variables. The goal is to capture the relationship between the two data sets with model of the form

$$\text{Pr}_{1h}(\text{foehn}) = f_{\text{learn}}(\text{ERA5}), \quad (3)$$

where the probability Pr_{1h} of the binary response is modeled as a function $f_{\text{learn}}()$ of the available information extracted from ERA5. $f_{\text{learn}}()$ can be any learner suitable for a binary response such as logistic regression, decision trees, random forests, or neural networks, to mention a few. For this study, three different learners/models are employed:

lasso Logistic regression with lasso (L1) regularization (Friedman, Hastie, and Tibshirani 2010; Tay, Narasimhan, and Hastie 2023).

stabsel Logistic regression with lasso-based stability selection (Meinshausen and Bühlmann 2010).

xgboost Extreme gradient boosting (Chen and Guestrin 2016).

In order to investigate the possible benefits of incorporating large-scale information from the stations’ neighborhood, two variations of each learner are considered: one utilizing the ‘full’ set of 497 variables and one only using the ‘direct’ set of 155 variables (Sec. 2.2).

To account for location and time of day, separate models are estimated for each of the six stations (Tab. 4) for each hour of the day (0000 UTC, 0100 UTC, . . . , 2300 UTC), resulting in a total of 864 models. Depending on the station, the training data for these models include 10–18 years of data (see Tab. 1). In addition, a six-fold cross-validation (CV) is performed using a fixed period of 12 years (2011–2022) where, in each fold, two consecutive years are left out as test data. Ellbögen and Innsbruck are missing one fold (with test data 2013–2014) where no measurements from the crest station are available and thus the classification is not possible.

3.3. Long-term foehn reconstruction

Once the models from the previous section are estimated, they can be applied to the entire ERA5 period available. Although this is a prediction from a statistical perspective, it is termed ‘reconstruction’ in this article, as these predictions are applied backwards in time. The result is an hourly time series of foehn probabilities $\widehat{\text{Pr}}_{1\text{h}}$ from January 1, 1940 to December 31, 2022 (83 years).

This reconstruction can fill possible gaps in historic records during the lifetime of an AWS and extend ‘foehn observations’ to times prior to or beyond the installation period of the AWS. The results may also serve as valuable input for investigating the effects of foehn, e.g., in ecology where the warming and drying effects of frequent foehn events can significantly impact flora and fauna or favor the occurrence of forest fires.

Moreover, the reconstruction offers the possibility to analyze foehn occurrence from a climatological perspective: Did the occurrence of foehn increase/decrease along with the changing climate over the decades? Are there changes in the seasonal or diurnal patterns? These questions are investigated in more detail in the next section.

3.4. Season-trend decomposition

The comprehensive reconstructed data set allows to study foehn occurrence in a climatological context. For this analysis, the hourly probability (Eqn. 3) is aggregated by (i) taking the highest probability $\widehat{\text{Pr}}_{1\text{h}}$ per day (0000 UTC–0000 UTC), before (ii) calculating monthly averages. The resulting time series contains “monthly means of the daily maxima”, which are then modeled using a season-trend decomposition.

Due to the nature of the data there is a large year-by-year but also within-year variability depending on the prevailing weather situation. To decompose the signal, a season-trend decomposition is employed separating the signal into long-term changes and a remainder component containing the residual variability.

In this study, the regression-based decomposition of [Dokumentov and Hyndman \(2022\)](#) is used, which also provides confidence intervals for the estimated season and trend components. The model for the monthly mean foehn probabilities y_t assumes an additive decomposition into a smoothly changing long-term trend T_t , a smoothly changing seasonal component $S_t^{(m)}$,

and a remainder R_t :

$$y_t = T_t + \sum_{m=1}^{12} S_t^{(m)} + R_t \quad \text{with } t \in 1, \dots, J, \quad (4)$$

where $m \in \{1, 12\}$ is the seasonal frequency (i.e., monthly) and J is the sample size (83 years \times 12 months = 996). The model is estimated via the R package `stR` (Dokumentov and Hyndman 2023).

4. Results

First, this section investigates which insights can be gained from the reconstruction about the foehn occurrence at the six different target stations. Different temporal scales are considered for this, namely: Inter-annual changes in the foehn probabilities in Section 4.1, long-term trends and seasonal patterns in Section 4.2, as well as changes in the diurnal patterns across decades in Section 4.3. All of these results are based on the reconstruction using the ‘lasso’ learner with the ‘full’ covariate set for the full time period (without cross-validation).

Second, the performance of the supervised learning model is assessed under different model specifications, namely: Using the ‘full’ set of all 497 variables vs. the 155 ‘direct’ variables only in Section 4.4 and comparing the performance of the three supervised learners (lasso, stability selection, extreme gradient boosting) in Section 4.5. All of these results are based on out-of-sample Brier scores obtained in a six-fold cross-validation.

4.1. Temporal changes: Average annual foehn probabilities

The primary outcome of this study is the complete reconstruction of hourly foehn probabilities over 83 years (see Sections 3.1–3.3), yielding time series with $N \sim 7.27 \cdot 10^5$ observations. To carve out inter-annual variations in the foehn probabilities, we aggregate the reconstructed data by taking the daily maximum of $\widehat{\text{Pr}}_{1h}$ (Eqn. 3) before calculating annual means. This can be interpreted as the average probability of observing a foehn event on any given day within that year.

Figure 4 contains the result for all six stations, with Ellbögen exhibiting the highest mean annual probabilities (on average 0.334), while Altdorf and Innsbruck show the lowest (on average 0.130 and 0.133 respectively). Additionally, the annual mean of daily maxima from the classification is shown for years with at least 80% of measurements available at the AWSs. The results show an overall good agreement between the two signals from the reconstruction and from the classification, with some larger gaps due to data availability as well as some noticeable differences for specific stations in particular years.

The reconstruction reveals a pronounced inter-annual variability, with certain years exhibiting a much higher annual mean than the long-term average, whilst others distinctly fall below. This variability is not random, as one can see similar patterns among the four south-foehn stations. For instance, all four stations show unusually high mean probabilities for 1951 and 1972. Similarly, the two north-foehn stations exhibit a similar temporal behavior over time.

Moreover, the figure suggests a possible increase in the annual mean foehn probability for south-foehn stations between 1940 and 1980. Hence this question is investigated in more detail in the next section.

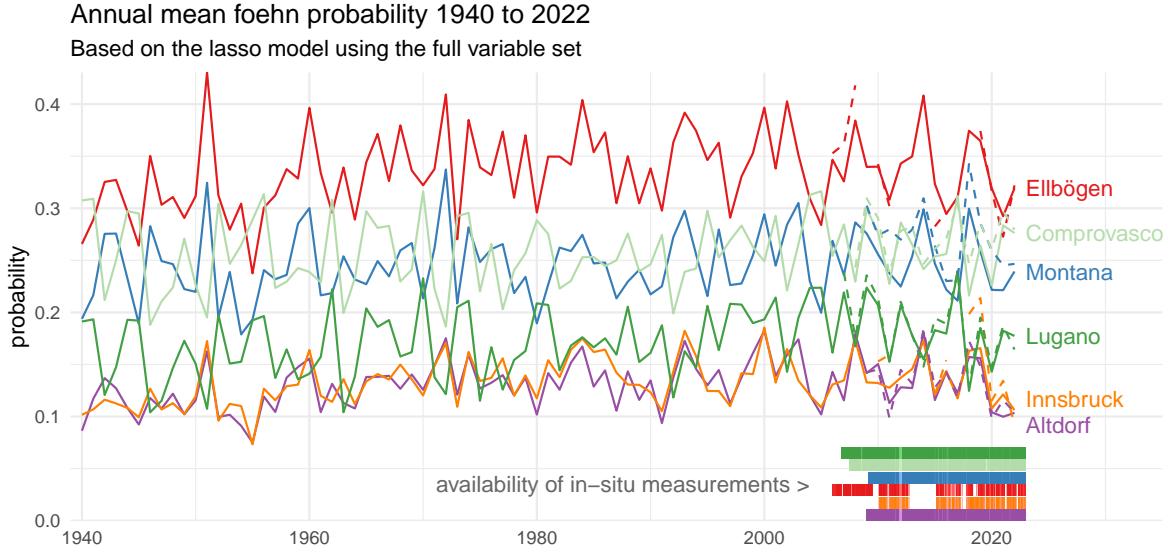


Figure 4: Annual mean of highest daily foehn probability (solid lines) for all six stations from 1940 to 2022 based on the ‘lasso’ model with ‘full’ covariate set. Additionally, annual means of daily maxima from the foehn classification using AWS data (dashed lines) and the availability of in-situ measurements (straight bands at the bottom) are shown. Appendix D shows a comparison to all other models and variants.

4.2. Temporal changes: Climatological trends and seasonal patterns

In this section, the analysis from the previous section is taken a step further. Rather than focusing on the inter-annual variation the goal is to bring out the long-term climatological trends and changes in the seasonal patterns. Hence the reconstructed hourly time series are again aggregated but to monthly (rather than annual) means of the daily maxima of $\widehat{\text{Pr}}_{1\text{h}}$. Based on the season-trend decomposition outlined in Section 3 Figure 5(a) illustrates the resulting smooth trends (T_t) along with the corresponding 95% confidence intervals. Figure 5(b) depicts the corresponding smoothly varying seasonal signals ($S_t^{(m)}$) averaged over decades for visual purposes (where decade 1940 corresponds to the years 1940–1949 etc.).

The estimated trends (Fig. 5a) show a significant increase for the two stations in Western Austria (Innsbruck, Ellbögen) between 1940 and 1980, and a plateau thereafter. All other stations show a linear increase over the study period. For four of the six stations (all except Montana and Comprovasco) the smooth trend differs significantly from a constant.

Figure 5(b) shows the analysis of the seasonal changes which reveals the different characteristics between north-foehn stations and south-foehn stations. The two stations located south of the main Alpine ridge, Comprovasco and Lugano, show one distinct maximum in spring and a minimum during autumn. This pattern is stable over the entire study period and no changes in the seasonal pattern ($S_t^{(m)}$) are found. The picture looks different when focusing on the four south-foehn stations which all show two maxima in spring and autumn with lower probability of foehn occurrence during summer and winter. Although not significant, the season-trend decomposition indicates an increase in the probability of foehn in spring (April, Mai) as well as in autumn (October, November) with a slight decrease in late summer

(August, September).

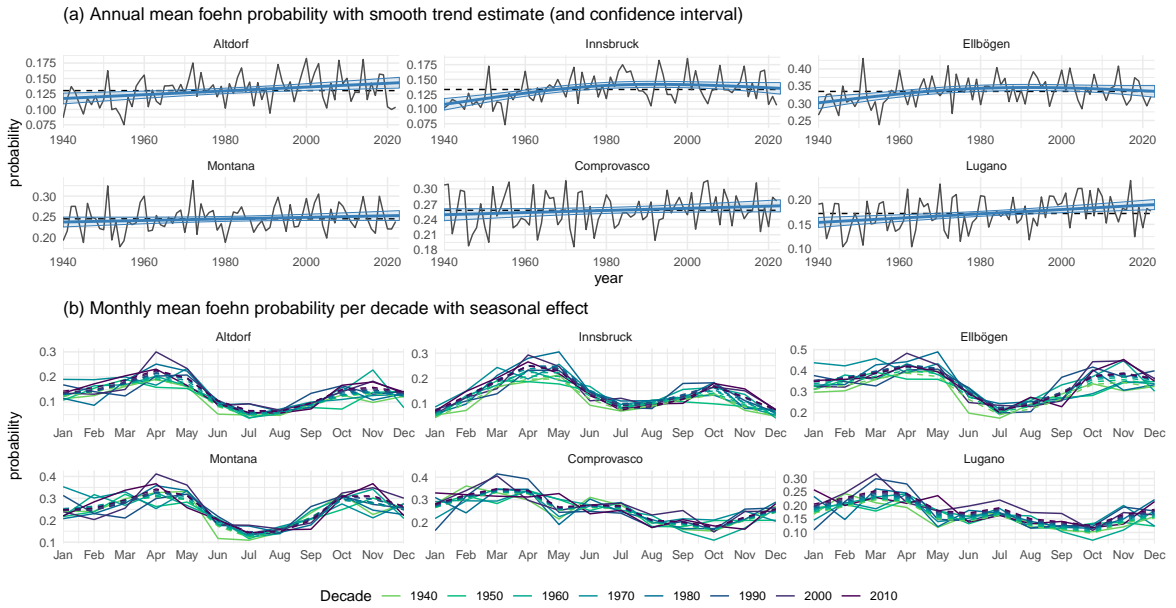


Figure 5: Results of the season-trend decomposition. (a) Estimated long-term trends with estimated 95% confidence interval (blue) on top of annual mean probabilities (black), the horizontal dashed line shows the mean of the trend for better orientation. (b) Estimated seasonal pattern averaged over the whole period 1940–2022 (dashed) and separately by decade (solid, label indicates first year of each decade).

4.3. Temporal changes: Intra-daily patterns

For certain applications, information about intra-daily patterns and their changes over time can be of great interest. With the hourly temporal resolution of the reconstruction, such insights are now possible across several decades.

Figure 6 shows Hovmöller diagrams for Ellbögen, depicting the decadal mean probability per time of day and month. Despite pronounced variability between the decades, the plot supports the previous findings showing an overall increase over time with strongest increase in spring (April, May) and in autumn (October, November). In addition, this visualization gives insights into the diurnal pattern. Generally, foehn occurrence in Ellbögen is more likely during the day (around 1000 UTC–2200 UTC) in spring and autumn, the period where indication for a certain increase was found (Sec. 4.2). The minimum average foehn probability is in the early morning and tied to the length of the night. The time of the minimum varies somewhat interdecadally.

4.4. Model performance: Benefit of full covariate set

As described in Section 3.2, two variants of the supervised learning methods are estimated: one using only the 155 ‘direct’ variables and one using the 497 ‘full’ variables including large-scale atmospheric conditions (Sec. 2.2). For both variants, a six-fold CV is performed (Sec. 3.2).

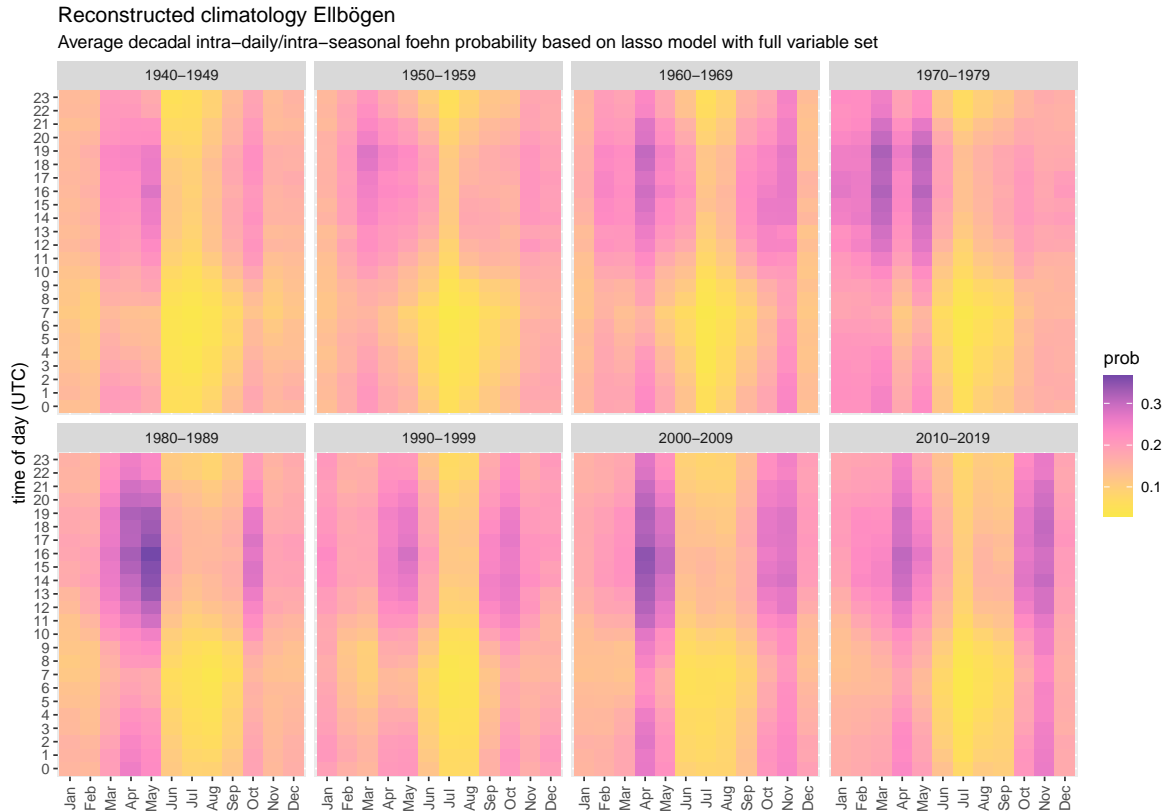


Figure 6: Hovmøller diagrams showing the average foehn probability for Ellbögen over the course of the day (y-axis) for all months (x-axis) for the decades 1940–2019.

To investigate the benefit of the ‘full’ covariate set, Figure 7 shows the Brier scores (BSs) for the ‘lasso’ model for all six stations. For each station and each variant, BSs are shown for the test data set (out-of-sample) as well as for the training data set (in-sample). This shows that the models based on the ‘full’ variable set clearly outperform the models based on the ‘direct’ variables only. Although the overall performance of the less complex models based on the ‘direct’ variable set is still decent, including the additional large-scale spatio-temporal information substantially improves the overall model performance.

In addition to the predictive skill, Figure 7 also shows the stability of the model with largest variance in the BSs visible on the test data sets in Ellbögen. On the training data sets the scores barely vary due to the large sample size (10 years, hourly data).

4.5. Model performance: Comparison of supervised learners

While the previous section focuses on the benefits of using more input data, this section compares the three different supervised learners described in Section 3.2. For simplicity, only the results for models based on the ‘full’ variable set are shown as they have been shown to outperform those only using the ‘direct’ variable set (Sec. 4.4).

Figure 8 illustrates that the BSs from the six-fold CV on the test set (out-of-sample) is comparable for all three supervised learners with only minor differences. The average BS is slightly

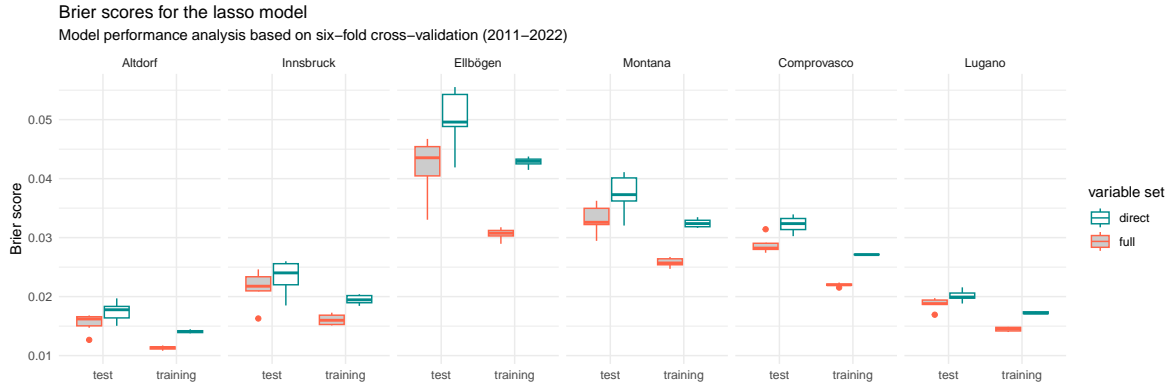


Figure 7: Comparison of ‘lasso’ model performance using the ‘direct’ variable set (blueish) versus the larger ‘full’ variable set (orange with gray filling) for all stations. Shown is the average Brier score from the six-fold CV for the test (out-of-sample) and training (ins-sample) period. Lower is better.

lower for ‘lasso’ (0.0261), followed by ‘stabsel’ (0.0276), and ‘xgboost’ (0.0283).

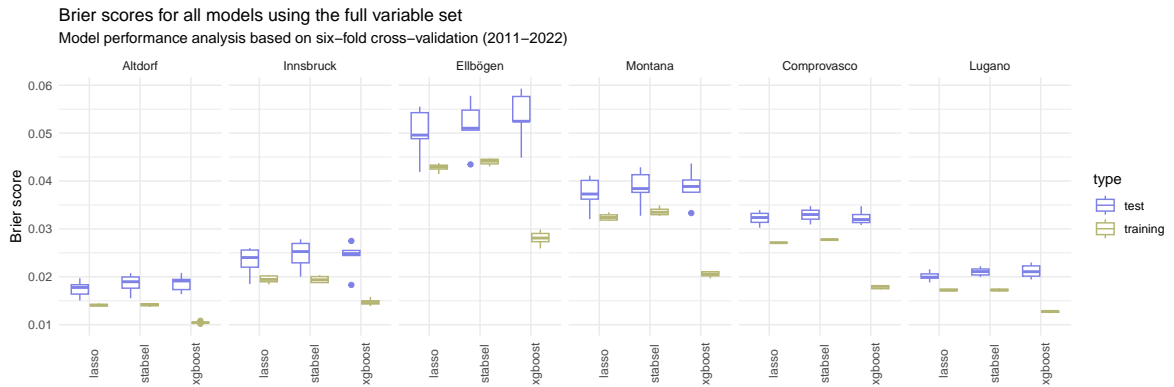


Figure 8: Comparison of all supervised learning models using the ‘full’ variable set. Brier scores for training (in-sample; green) and test (out-of-sample; violet) data set based on six-fold cross-validation. Lower is better.

On the training data (in-sample) the picture is similar for ‘lasso’ and ‘stabsel’ but ‘xgboost’ has much lower BSs. This indicates that ‘xgboost’ might be subject to some overfitting, despite careful tuning of the hyperparameters (App. C.3).

5. Discussion and outlook

Using a novel combination of unsupervised and supervised learning we are able to accurately reconstruct long-term foehn time series (starting from 1940) at hourly resolution. More specifically, foehn classification is first accomplished by (unsupervised) Gaussian finite mixture models based on AWS measurements and then linked to ERA5 data using binary supervised learners such as lasso, stability selection, or extreme gradient boosting. The resulting foehn reconstruction enables novel analyses, exemplified here by investigating long-term changes in

trends, seasonal patterns, and diurnal cycles of foehn occurrence.

The season-trend decomposition based on the period 1940–2022 reveals that all six stations considered have either experienced a linear increase in foehn occurrence (probability) over the entire study period or an increase between 1940 and the early 1980s that leveled off afterwards. For four of the six stations it can be shown that this increase is significant. Although no significant change in the seasonality is found, the results for all south-foehn stations (Altdorf, Montana, Ellbögen, and Innsbruck) indicate a slight increase in the occurrence of foehn in spring and autumn, with a slight decrease in late summer.

The high quality of the foehn reconstruction is partially due to using a large set of predictor covariates that not only contains information at the target location but also includes additional large-scale atmospheric information from the stations’ surrounding. The benefits of this full set of covariates are similar for all three supervised learners considered: logistic regression with lasso regularization (‘lasso’), logistic-regression-based stability selection (‘stabsel’), and extreme gradient boosting (‘xgboost’). Lasso performs best in our application, closely followed by the other two learners. Some further improvements might be gained for xgboost if overfitting on the training data can be further reduced, e.g., by a different hyperparameter tuning strategy.

For a comparison to existing publications, we complement the Brier scores shown in the main paper by other popular scores for binary outcomes, such as the false negative rate (FNR, also known as miss rate), false positive rate (FPR, also known as false alarm rate), and percent correct (PC, also known as accuracy). Based on the best model (lasso with full covariate set), we obtain the following performances for Altdorf: 15.7%/0.4%/98.8% (FNR/FPR/PC). These align well with the existing literature and stand out for an exceptionally low FPR. [Sprenger *et al.* \(2017\)](#) report 11.8%/33.8%/96.5% and [Mony *et al.* \(2021\)](#) report 21.4%/21.4%/97.7%. Similarly for Lugano we obtain 15.3%/0.7%/98.2%, while [Mony *et al.* \(2021\)](#) report 22.1%/22.1%/97.1%. More details are included in the appendix (App. E).

The same holds for the foehn classification when compared to existing literature and the Swiss foehn index (SFI) operationally used at MeteoSwiss in terms of “average foehn hours per year”. The results from the Gaussian mixture model (Sec. 3.1) for Altdorf show an average of 482.4 h/year which aligns well with the SFI (458.4 h/year), as well as the results reported by [Dürr \(2008\)](#) (478 h/year), [Jansing *et al.* \(2022\)](#) (465.8 h/year), and [MeteoSwiss \(2024\)](#) (477 h/year). Montana exhibits 1007.4 h/year (SFI 904.7 h/year¹), while Lugano and Comprovasco show 644.7 h/year (SFI 563.0 h/year, [MeteoSwiss \(2024\)](#) 551 h/year) and 1077.4 h/year (SFI 953.4 h/year), respectively.

It should be emphasized that the excellent performance of the combined approach depends crucially on the high quality of the automatic foehn classification in the Gaussian finite mixture model. Thus, if the separation of the AWS measurements into ‘foehn’ or ‘no foehn’ components works well (as for the six stations presented), then different binary supervised learners are able to link this reliably to the ERA5 data. However, there may also be stations where a distinction into just two components might not be sufficient. For example, we have found this to be the case for Aigle, Switzerland, where a three-component mixture model appears to be necessary to separate light down-valley winds, strong humid (catabatic) outflows, and actual foehn situations (details not shown).

¹Average based on the years 2009–2016 only.

Computational details

The results in this paper were obtained using R 4.2+. The majority of data preparation and handling is done using the R packages **stars** 0.6.4, **sf** 1.0.15 and **zoo** 1.8.12. **foehnix** 0.1.6 is used for foehn classification, the supervised learning is based on **glmnet** 4.1.7 and **xgboost** 1.7.5.1. The season-trend decomposition is based on the R package **stR** 0.6.

Acknowledgments

The study is partly based on the preliminary work of [Morgenstern \(2020\)](#). The computational results presented here have been achieved (in part) using the LEO HPC infrastructure of the University of Innsbruck.

References

- Armi L, Mayr GJ (2007). “Continuously Stratified Flows Across an Alpine Crest with a Pass: Shallow and Deep Föhn.” *Quarterly Journal of the Royal Meteorological Society*, **133**(623), 459–477. doi:10.1002/qj.22.
- Armi L, Mayr GJ (2011). “The Descending Stratified Flow and Internal Hydraulic Jump in the Lee of the Sierras.” *Journal of Applied Meteorology and Climatology*, **50**(10), 1995–2011. doi:10.1175/JAMC-D-10-05005.1.
- Cape MR, Vernet M, Skvarca P, Marinsek S, Scambos T, Domack E (2015). “Foehn Winds Link Climate-Driven Warming to Ice Shelf Evolution in Antarctica.” *Journal of Geophysical Research: Atmospheres*, **120**(21), 11037–11057. doi:10.1002/2015JD023465.
- Chen T, Guestrin C (2016). “XGBoost: A Scalable Tree Boosting System.” In *Proceedings of the 22nd ACM SIGKDD International Conference on Knowledge Discovery and Data Mining*, KDD ’16, pp. 785–794. Association for Computing Machinery, New York, NY, USA. ISBN 9781450342322. doi:10.1145/2939672.2939785.
- Chen T, He T, Benesty M, Khotilovich V, Tang Y, Cho H, Chen K, Mitchell R, Cano I, Zhou T, Li M, Xie J, Lin M, Geng Y, Li Y, Yuan J (2023). *xgboost: Extreme Gradient Boosting*. R package version 1.7.5.1, URL <https://CRAN.R-project.org/package=xgboost>.
- Courvoisier H, Gutermann T (1971). “Zur praktischen Anwendung des Föhntests von Widmer.” **21**, 7pp. Accessed 2024-03-21, URL http://www.agfoehn.org/doc/Courvoisier_1971.pdf.
- Datta RT, Tedesco M, Fettweis X, Agosta C, Lhermitte S, Lenaerts JTM, Wever N (2019). “The Effect of Foehn-Induced Surface Melt on Firn Evolution over the Northeast Antarctic Peninsula.” *Geophysical Research Letters*, **46**(7), 3822–3831. doi:10.1029/2018GL080845.
- Dokumentov A, Hyndman RJ (2022). “STR: Seasonal-Trend Decomposition Using Regression.” *INFORMS Journal on Data Science*, **1**(1), 50–62. doi:10.1287/ijds.2021.0004.
- Dokumentov A, Hyndman RJ (2023). *stR: STR Decomposition*. R package version 0.6, URL <https://CRAN.R-project.org/package=stR>.

- Dürr B (2008). “Automatisiertes Verfahren zur Bestimmung von Föhn in Alpentälern.” *Arbeitsbericht*, MeteoSchweiz. Accessed 2024-03-21, URL <https://www.meteoschweiz.admin.ch/dam/jcr:1fbe0d4e-fc7c-4121-b89e-1429a931272f/ab223.pdf>.
- Elvidge AD, Kuipers Munneke P, King JC, Renfrew IA, Gilbert E (2020). “Atmospheric Drivers of Melt on Larsen C Ice Shelf: Surface Energy Budget Regimes and the Impact of Foehn.” *Journal of Geophysical Research: Atmospheres*, **125**(17), e2020JD032463. doi: [10.1029/2020JD032463](https://doi.org/10.1029/2020JD032463).
- Francis D, Fonseca R, Mattingly KS, Lhermitte S, Walker C (2023). “Foehn Winds at Pine Island Glacier and Their Role in Ice Changes.” *The Cryosphere*, **17**(7), 3041–3062. doi: [10.5194/tc-17-3041-2023](https://doi.org/10.5194/tc-17-3041-2023).
- Friedman JH, Hastie T, Tibshirani R (2010). “Regularization Paths for Generalized Linear Models via Coordinate Descent.” *Journal of Statistical Software*, **33**(1), 1–22. doi: [10.18637/jss.v033.i01](https://doi.org/10.18637/jss.v033.i01).
- Grün B, Leisch F (2008). “FlexMix Version 2: Finite Mixtures with Concomitant Variables and Varying and Constant Parameters.” *Journal of Statistical Software*, **28**(4), 1–35. doi: [10.18637/jss.v028.i04](https://doi.org/10.18637/jss.v028.i04).
- Gutermann T, Dürr B, Richner H, Bader S (2012). “Föhnklimatologie Altdorf: Die lange Reihe (1864–2008) und ihre Weiterführung, Vergleich mit anderen Stationen.” *Fachbericht MeteoSchweiz*, **241**, 1–53. Accessed 2024-03-21, URL <https://www.meteoswiss.admin.ch/services-and-publications/publications/reports-and-bulletins/2012/foehnklimatologie-altorf--die-lange-reihe--1864-2008--und-ihre-.html>.
- Hersbach H, Bell B, Berrisford P, Biavati G, Horányi A, Muñoz Sabater J, Nicolas J, Peubey C, Radu R, Rozum I, Schepers D, Simmons A, Soci C, Dee D, Thépaut JN (2023a). “ERA5 Hourly Data on Pressure Levels from 1940 to Present.” doi: [10.24381/cds.bd0915c6](https://doi.org/10.24381/cds.bd0915c6). Accessed 2024-03-21.
- Hersbach H, Bell B, Berrisford P, Biavati G, Horányi A, Muñoz Sabater J, Nicolas J, Peubey C, Radu R, Rozum I, Schepers D, Simmons A, Soci C, Dee D, Thépaut JN (2023b). “ERA5 Hourly Data on Single Levels from 1940 to Present.” doi: [10.24381/cds.adbb2d47](https://doi.org/10.24381/cds.adbb2d47). Accessed 2024-03-21.
- Jansing L, Papritz L, Dürr B, Gerstgrasser D, Sprenger M (2022). “Classification of Alpine South Foehn based on 5 Years of Kilometre-Scale Analysis Data.” *Weather and Climate Dynamics*, **3**(3), 1113–1138. doi: [10.5194/wcd-3-1113-2022](https://doi.org/10.5194/wcd-3-1113-2022).
- Laffin MK, Zender CS, Singh S, Van Wessem JM, Smeets CJPP, Reijmer CH (2021). “Climatology and Evolution of the Antarctic Aeninsula Föhn Wind-Induced Melt Regime From 1979–2018.” *Journal of Geophysical Research: Atmospheres*, **126**(4), 1–19. doi: [10.1029/2020JD033682](https://doi.org/10.1029/2020JD033682).
- Mayr GJ, Armi L (2008). “Föhn as a Response to Changing Upstream and Downstream Air Masses.” *Quarterly Journal of the Royal Meteorological Society*, **134**(635), 1357–1369. doi: [10.1002/qj.295](https://doi.org/10.1002/qj.295).

- Meinshausen N, Bühlmann P (2010). “Stability Selection.” *Journal of the Royal Statistical Society B*, **72**(4), 417–473. doi:10.1111/j.1467-9868.2010.00740.x.
- MeteoSwiss (2024). “Wetter und Klima A bis Z: Föhnhäufigkeit.” Accessed 2024-03-21, URL <https://www.meteoschweiz.admin.ch/wetter/wetter-und-klima-von-a-bis-z/foehnhaeufigkeit.html>.
- Mony C, Jansing L, Sprenger M (2021). “Evaluating Foehn Occurrence in a Changing Climate Based on Reanalysis and Climate Model Data Using Machine Learning.” *Weather and Forecasting*, **36**(6), 2039–2055. doi:10.1175/WAF-D-21-0036.1.
- Morgenstern DS (2020). *Multidecadal Foehn Time Series Reconstruction Using Machine Learning and ERA5 Reanalysis Data*. Master’s thesis, Universität Innsbruck. URL <https://bibsearch.uibk.ac.at/AC15677542>.
- Plavcan D, Mayr GJ (2015). “Towards an Alpine Foehn Climatology.” 33rd International Conference on Alpine Meteorology, Innsbruck. Accessed 2024-03-21, URL https://www.uibk.ac.at/congress/icam2015/abstracts_oral_presentations.htm#014.4.
- Plavcan D, Mayr GJ, Zeileis A (2014). “Automatic and Probabilistic Foehn Diagnosis with a Statistical Mixture Model.” *Journal of Applied Meteorology and Climatology*, **53**(3), 652–659. doi:10.1175/JAMC-D-13-0267.1.
- Reinhard M, Rebetez M, Schlaepfer R (2005). “Recent Climate Change: Rethinking Drought in the Context of Forest Fire Research in Ticino, South of Switzerland.” *Theoretical and Applied Climatology*, **82**(1), 17–25. doi:10.1007/s00704-005-0123-6.
- Richner H, Hächler P (2013). *Understanding and Forecasting Alpine Foehn*, chapter 4, pp. 219–260. Springer-Verlag, Dordrecht. ISBN 978-94-007-4098-3. doi:10.1007/978-94-007-4098-3_4.
- Schoennagel T, Veblen TT, Romme WH (2004). “The Interaction of Fire, Fuels, and Climate across Rocky Mountain Forests.” *BioScience*, **54**(7), 661–676. doi:10.1641/0006-3568(2004)054[0661:TIOFFA]2.0.CO;2.
- Speirs JC, McGowan HA, Steinhoff DF, Bromwich DH (2013). “Regional Climate Variability Driven by Foehn Winds in the McMurdo Dry Valleys, Antarctica.” *International Journal of Climatology*, **33**(4), 945–958. doi:10.1002/joc.3481.
- Sprenger M, Schemm S, Oechslin R, Jenkner J (2017). “Nowcasting Foehn Wind Events Using the AdaBoost Machine Learning Algorithm.” *Weather and Forecasting*, **32**(3), 1079–1099. doi:10.1175/WAF-D-16-0208.1.
- Stauffer R (2023). “foehnix: A Toolbox for Automated Foehn Classification based on Mixture Models.” R package version 0.1.6, URL <https://retostauffer.github.io/Rfoehnix/>.
- Tay JK, Narasimhan B, Hastie T (2023). “Elastic Net Regularization Paths for All Generalized Linear Models.” *Journal of Statistical Software*, **106**(1), 1–31. doi:10.18637/jss.v106.i01.

Turton JV, Kirchgaessner A, Ross AN, King JC (2018). “The Spatial Distribution and Temporal Variability of Föhn Winds over the Larsen C Ice Shelf, Antarctica.” *Quarterly Journal of the Royal Meteorological Society*, **144**(713), 1169–1178. doi:10.1002/qj.3284.

Wessen JMV, Laffin MK (2022). “Regional Atmospheric Climate Model 2 (RACMO2), version 2.3p2.” doi:10.5281/zenodo.3677641. Accessed 2023-08-23.

Widmer R (1966). “Statistische Untersuchungen über den Föhn im Reusstal und Versuch einer objektiven Föhnprognose für die Station Altdorf.” *Vierteljahresschrift der Naturforschenden Gesellschaft Zürich*, **111**, 331–375. Accessed 2024-03-21, URL https://www.ngzh.ch/archiv/1966_111/111_3-4/111_20.pdf.

Zumbrunnen T, Bugmann H, Conedera M, Bürgi M (2009). “Linking Forest Fire Regimes and Climate – A Historical Analysis in a Dry Inner Alpine Valley.” *Ecosystems*, **12**(1), 73–86. doi:10.1007/s10021-008-9207-3.

A. ERA5 fields

As described in Section 2.2 information from 90 different ERA5 fields is bilinearly interpolated to (i) the target location of the different stations used (cf. 2.1) as well as to a series of neighboring points arranged in a ‘star’ formation to include large-scale information. The fields used are listed in Table 2 and 3.

CDS ERA5 fields name	
100m_u_component_of_wind	100m_v_component_of_wind
10m_u_component_of_wind	10m_v_component_of_wind
10m_wind_gust_since_previous_post_processing	instantaneous_10m_wind_gust
2m_dewpoint_temperature	2m_temperature
surface_pressure	mean_sea_level_pressure
eastward_gravity_wave_surface_stress	northward_gravity_wave_surface_stress
convective_precipitation	large_scale_precipitation
total_precipitation	boundary_layer_dissipation
boundary_layer_height	charnock
friction_velocity	gravity_wave_dissipation
high_cloud_cover	low_cloud_cover
medium_cloud_cover	total_cloud_cover
total_column_cloud_liquid_water	surface_net_solar_radiation
surface_net_thermal_radiation	surface_sensible_heat_flux
surface_solar_radiation_downwards	surface_thermal_radiation_downwards

Table 2: List of ERA5 single level field retrieved.

CDS ERA5 fields name	
divergence	geopotential
potential_vorticity	specific_humidity
temperature	u_component_of_wind
v_component_of_wind	vertical_velocity
specific_cloud_liquid_water_content	vorticity

Table 3: List of ERA5 pressure level fields retrieved; each on the standard pressure levels 500 hPa, 700 hPa, 750 hPa, 800 hPa, 850 hPa and 900 hPa.

To keep the approach generic, these neighbouring points are ‘arbitrary’ points not linked to stations or cities, but geometrically placed around the target station relative to its location to the main mountain range. Figure 2 (main article) shows these ‘stars’ which are constructed as follows: First, the orthogonal from the center location (station location; C) to the main mountain range is computed. Along this orthogonal axis, two additional points upwind of the foehn wind direction (U, UU) and two points in the downwind direction (D, DD) are defined with a radius of 1° and 2° from the center point. Second, four points with a radius of 2° from the center point deviating by 45° from the orthogonal are added, defining points on the right hand side (*R) and left hand side (*L) of the main foehn direction in the upwind direction (UR, UL) and downwind direction (DR, DL). The downwind direction for stations located north of the main alpine range is towards north (south-foehn stations), for those located south of the main alpine range the downwind direction is toward south (north-foehn stations).

Based on these points, the ‘direct’ variable set (155 variables) as well as the ‘full’ variable set (497 variables) are calculated as described in Section 2.2 (main article). The extended (‘full’) variable set contains a series of spatial and spatio-temporal information such as:

- surface pressure differences between C to U, U to C, UL to DR and others,
- potential temperature differences between C to U, U to C, UL to DR and others,
- differences in vertical temperature differences between C to U, U to C, UL to DR and others,
- sum of precipitation on the upwind side (sum of U, UU, UR, UL) as well as on the downwind side (sum of D, DD, DR, DL) as well and the difference between these two sums,
- mean cloud cover on the upwind side (sum of U, UU, UR, UL) as well as on the downwind side (sum of D, DD, DR, DL) as well and the difference between these two means.

Moreover, temporal variables are calculated including e.g., changes in the geopotential height, temperature, or changes in humidity on different levels over the past 3 hours or over the next 3 hours and variations thereof.

B. Unsupervised learning: Two-component mixture model

For all eight AWSs used (Tab. 1; main article) observations are available for the most recent 10–18 years on a 10 min temporal resolution. Since foehn winds show a characteristic wind direction, only observations meeting a specific precondition are used for classification as described in Section 3.1. Table 4 shows the wind sectors used for each target site, as well as the amount of data used for classification.

The (conditional) two-component Gaussian mixture model with concomitant variables Grün and Leisch (2008); Plavcan *et al.* (2014); Stauffer (2023) is defined as follows:

$$h(\mathbf{y}, \mathbf{X}, \theta, \alpha) = \underbrace{(1 - \pi(\mathbf{X}, \alpha)) \cdot \mathcal{N}(\mathbf{y}, \theta_1)}_{\text{first component}} + \underbrace{\pi(\mathbf{X}, \alpha) \cdot \mathcal{N}(\mathbf{y}, \theta_2)}_{\text{second component}},$$

where the joint (mixed) density $h()$ is the sum of two Gaussian components $\mathcal{N}()$ times the probability $\pi()$ that an observation falls into the second component. The potential temperature \mathbf{y} is used to separate the two components with θ_\bullet representing the distribution parameters of $\mathcal{N}()$. The concomitant model modeling π is a logistic regression model employing an intercept as well as relative humidity and wind speed (\mathbf{X}) and can be written as:

$$\log\left(\frac{\pi}{1 - \pi}\right) = \mathbf{X}^\top \alpha; \quad \pi = \frac{\exp(\mathbf{X}^\top \alpha)}{1 + \exp(\mathbf{X}^\top \alpha)}.$$

Once the required parameters θ, α are estimated, the final a-posteriori probability $\hat{p} \in [0, 1]$ can be calculated using

$$\hat{p}(\mathbf{y}, \mathbf{X}, \theta, \alpha) = \frac{\pi(\mathbf{X}, \alpha) \cdot \mathcal{N}(\mathbf{y}, \theta_2)}{(1 - \pi(\mathbf{X}, \alpha)) \cdot \mathcal{N}(\mathbf{y}, \theta_1) + \pi(\mathbf{X}, \alpha) \cdot \mathcal{N}(\mathbf{y}, \theta_2)}$$

The result is the probability $\hat{p}(\mathbf{y}, \mathbf{X}, \theta, \alpha) = Pr_{\text{obs}}(\text{foehn})$ (Eqn. 1) with the same temporal resolution as the in-situ observations. After the temporal upscaling (Sec. 3.1) this result used to label the data as ‘foehn’ or ‘no foehn’ event (Pr_{1h} ; Eqn. 2).

	Stations, conditional wind direction, data used
Altdorf	Valley station: Altdorf (60°–240°) Crest station: Gütsch, Andermatt (105°–285°) 20.0 % within sector, 57.1 % outside sector, 22.9 % removed
Innsbruck	Valley station: Universität Innsbruck (130°–230°) Crest station: Sattelberg (90°–270°) 5.8 % within sector, 49.3 % outside sector, 44.9 % removed
Ellbögen	Valley station: Ellbögen (45°–225°) Crest station: Sattelberg (90°–270°) 22.6 % within sector, 49.0 % outside sector, 28.4 % removed
Montana	Valley station: Montana (30°–100°) Crest station: Gütsch, Andermatt (120°–180°) 23.2 % within sector, 52.9 % outside sector, 23.9 % removed
Comprovasco	Valley station: Comprovasco (270°–30°) Crest station: Gütsch, Andermatt (290°–89°) 33.5 % within sector, 51.2 % outside sector, 15.4 % removed
Lugano	Valley station: Lugano (270°–80°) Crest station: Gütsch, Andermatt (290°–89°) 26.9 % within sector, 62.1 % outside sector, 10.9 % removed

Table 4: Overview of the stations and defined wind sectors used as precondition for classification. For each target location (left column) the corresponding valley station and crest station and their required wind sectors are listed. In addition, the percentage of observations used for classification (within sector), not used in classification (outside sector) and removed due to missing data is shown (based on all available data). More station details cf. Table 1.

C. Supervised learning: Reconstruction

The hourly labeled data (Sec. 3.1, App. B) are combined with the hourly data derived from ERA5 (Sec. 2.2, App. A), serving the training data for the supervised learning.

C.1. lasso: Logistic regression with lasso (L1) regularization

Due to the large number of possible covariates from ERA5 and the fact that many of these variables are highly correlated, penalization is required. This study employs lasso (least absolute shrinkage and selection operator) with L1 regularization, optimizing the following penalized log-likelihood:

$$(\hat{\beta}_0, \hat{\beta}) = \operatorname{argmin}_{(\beta_0, \beta) \in \mathcal{R}^k} \left[\frac{1}{2N} \sum_{i=1}^N (\operatorname{Pr}_{\text{obs}, i} - \beta_0 - \text{ERA5}^\top \beta)^2 + \lambda \|\beta\|_1 \right], \quad (5)$$

with $\text{ERA5} \in \mathcal{R}^{N \times k}$, where N is the number of hourly foehn probabilities (Sec. 3.1) and k the number of available covariates (Sec. 2.2).

To find the optimal tuning parameter $\hat{\lambda}$, a 30-fold cross-validation is performed which yields the optimal (regularized) set of regression coefficients $\hat{\beta}_0, \hat{\beta}$ using the *R* package `glmnet` (with `s = "lambda.min"`).

C.2. stabsel: Logistic regression with lasso-based stability selection

As the lasso penalty shrinks more and more parameters to 0 with increasing λ , this model can also be used for stability selection (Meinshausen and Bühlmann 2010). The penalized regression model is estimated M times for a series of values $\lambda \in [0, \infty]$. The first K parameters which enter the model ($\neq 0$) will be memorized.

In this study, this is repeated $M = 200$ times, estimating the model on a random subset with only 50% of the available data. As the number of ‘foehn’ events can be rather low (0.6%–29% depending on station/time of day) a stratified random subset (bagging) is drawn each time containing the same proportion of ‘foehn’ and ‘no foehn’ events as the full data set. In each of the $M = 200$ iterations, the name of the first $K = 40$ covariates entering the model is stored. Those covariates which have been selected more than 60% of the time (at least 121/200 times) are then used to estimate an additional unregularized logistic regression model.

1. Whilst iteration is ≤ 200 :
 - (a) Draw stratified subsample of size $N/2$
 - (b) Estimate regularized coefficients $(\hat{\beta}_0, \hat{\beta})$ for different λ s
 - (c) Extract and keep the name of the first $K = 40$ covariates entering the model
2. Select the covariates which a selection frequency > 0.6
3. Estimate final (unregularized) logistic regression model with the covariates from Step 2

Stability selection allows to automatically identify the most important covariates among the ones available and to strongly reduce the complexity of the final model (Step 3) without losing much predictive performance.

C.3. xgboost: Extreme gradient boosting

Extreme gradient boosting (XGBoost; Chen and Guestrin 2016) is a supervised machine learning algorithm using a series of decision trees to best predict the labeled data (response) using a series of explanatory variables (covariates). Similar to random forests, XGBoost uses estimates and combines a series of decision trees (a weak learner). The main difference is that XGBoost uses a gradient decent method (thus the name) by optimizing the model based on the outcome of the previous tree by finding additional split points to improve the objective function.

Overly simplified, XGBoost starts with estimating one decision tree and evaluates its residuals (i.e., the yet unexplained part/misclassified data). These residuals are then used as input for the next iteration to estimate a new tree to improve the misclassification from the previous step.

A series of tuning parameters exist such as the number of iterations to be performed, the maximum depth of an individual tree, or the learning rate to update the parameters in each iteration. Choosing these tuning parameters wrong can lead to overly conservative models (not flexible enough) or models which overfit the data, both of which can result in a poor (out-of-sample) predictive performance. One way to avoid these scenarios is to perform proper cross-validation. We performed a (limited) grid search using the *R* package `xgboost` (Chen *et al.* 2023) with the following parameter space:

- `eta`, learning rate: {0.1, 0.125, 0.15, 0.2}
- `max_depth`, maximum depth of each weak learner (tree): {5, 10, 20}
- `min_child_weight`, minimum sum of instance weight needed in a child: {2, 4, 6}
- `gamma`, minimum loss reduction required: {2, 5, 10}

This yields an overall number of 108 unique combinations. For each combination, a 10-fold cross-validation using random stratified subsamples and a maximum of 20 boosting iterations is performed. It is then evaluated which parameter set and boosting iteration resulting in the lowest average out-of-sample error to estimate one final model using all data. A summary of the selected tuning parameters is shown in Table 5. All models are estimated using the ‘gbtree’ booster and the binomial logistic objective function.

	mean	median	range
subsample	0.500	0.5	0.5-0.5
eta	0.200	0.2	0.2-0.2
max_depth	11.602	10	5-20
min_child_weight	3.423	4	2-6
gamma	2.868	2	2-10
nround	19.997	20	19-20

Table 5: Mean, median and range of the selected XGBoost parameters via stratified 10-fold cross-validation over all stations and times of the day using the ‘full’ variable set.

D. Long-term reconstruction

Figure 4 (main article, Sec 4.1) only shows results of the reconstruction based on the ‘lasso’ model with the ‘full’ variable set. Figure 9 shows the same information for all six stations including the results of all three models (lasso, stabsel, xgboost) and both variants using either the ‘direct’ variable set or ‘full’ variable set.

The results of these six versions (three models, two variants each) show differences but agree in large parts, showing similar features across the years.

E. Model performance/model comparison

Analogous to Figures 7 and 8 (main article; Sec, 4.4 & 4.5) Figure 10 shows average Brier scores from six-fold CV for all three models and model variants (using the ‘direct’ or ‘full’ variable set). As discussed in the main article, the ‘xgboost’ model might be subject to some overfitting (training) as it always shows lowest scores across all stations and both model variants.

In addition, event-based metrics are used in the discussion (Sec 5) to compare the results of this study to existing literature. Table 6 contains the results for all six stations and both model variants (‘direct’/‘full’ variable set) for all three supervised methods (‘lasso’/‘stabsel’/‘xgboost’).

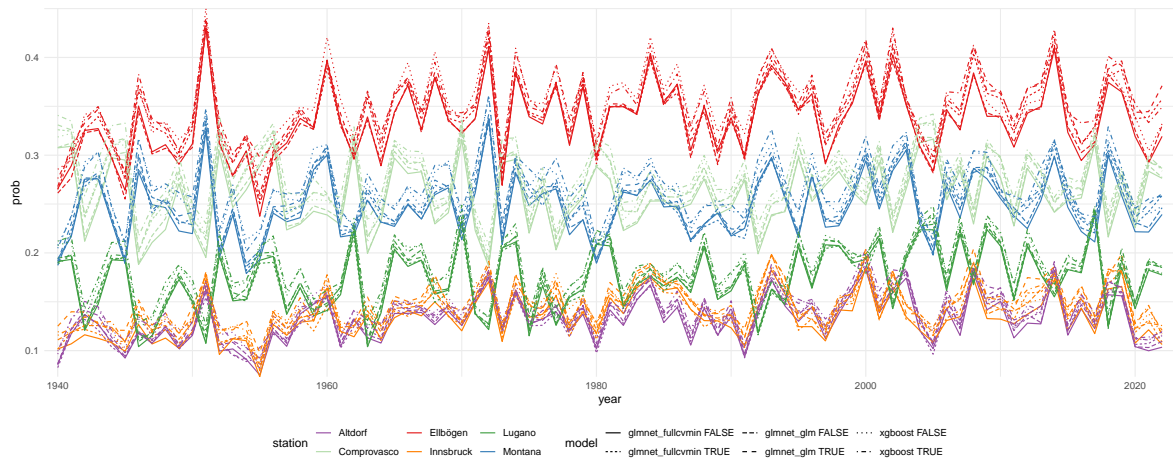


Figure 9: Annual mean of daily maxima as in Figure 4 for all stations, all three models in both variants.

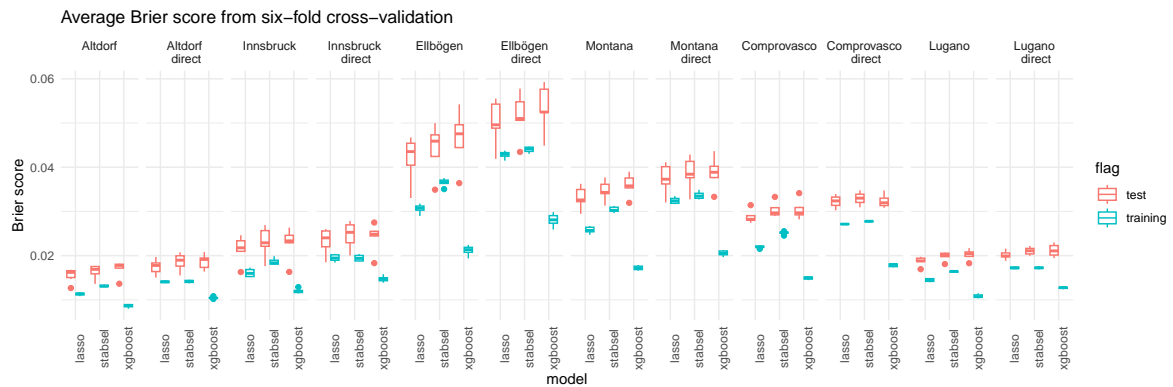


Figure 10: Comparison of average Brier score of all models (lasso, stabsel, xgboost) and variants ('direct'/'full') for all six stations. Average scores of the six-fold CV are displayed for the test (red) and training (green) period.

Affiliation:

Reto Stauffer
 Universität Innsbruck
 Faculty of Economics and Statistics
 and Digital Science Center
 Universitätsstr. 15
 6020 Innsbruck, Austria
 E-mail: Reto.Stauffer@uibk.ac.at

Station	Variable set	FNR	FPR	PC
Altdorf	direct	20.0/18.9/13.6	0.6/0.7/0.3	98.4/98.3/99.0
	full	15.7/17.1/10.7	0.4/0.6/0.2	98.8/98.5/99.2
Innsbruck	direct	42.9/40.6/31.7	0.6/0.8/0.3	97.6/97.6/98.4
	full	37.2/36.1/24.0	0.5/0.8/0.2	98.0/97.8/98.8
Ellbögen	direct	19.4/19.9/12.9	2.9/3.0/1.6	94.2/94.0/96.4
	full	13.9/15.9/7.9	1.9/2.4/1.0	96.0/95.3/97.8
Montana	direct	24.1/24.4/14.5	1.7/1.9/0.8	95.7/95.5/97.6
	full	19.4/21.7/12.1	1.3/1.8/0.7	96.6/95.9/98.0
Comprovasco	direct	17.4/17.6/10.3	1.7/1.8/0.9	96.4/96.3/97.9
	full	13.7/15.3/8.4	1.3/1.6/0.7	97.2/96.7/98.4
Lugano	direct	17.2/17.3/11.8	0.9/1.0/0.5	97.9/97.8/98.6
	full	15.3/16.4/9.5	0.7/0.9/0.4	98.2/97.9/99.0

Table 6: Miss rate (FNR), false alarm rate (FPR) and percent correct (PC) in percent based on the entire period (in-sample) for model comparison. Scores are shown for the ‘lasso’/‘stabsel’/‘xgboost’ models in this order.